ISSN 1674-1056
http://cpb.iphy.ac.cn
http://iopscience.iop.org/cpb
中国物理 B
Chinese Physics
中国物理
Chinese Physics B

High-performance inverters based on ambipolar organic-inorganic heterojunction thin-film transistors

Sheng Sun(孙圣), Yuzhi Li(李育智), Shengdong Zhang(张盛东)

Citation: Chin. Phys. B . 2020, 29(5): 058503 . **doi:** 10.1088/1674-1056/ab7e96
Journal homepage: http://cpb.iphy.ac.cn; http://iopscience.iop.org/cpb

What follows is a list of articles you may be interested in

Effects of buried oxide layer on working speed of SiGe heterojunction photo-transistor

Xian-Cheng Liu(刘先程), Jia-Jun Ma(马佳俊), Hong-Yun Xie(谢红云), Pei Ma(马佩), Liang Chen(陈亮), Min Guo(郭敏), Wan-Rong Zhang(张万荣)

Chin. Phys. B . 2020, 29(2): 028501 . **doi:** 10.1088/1674-1056/ab5f01

High-throughput fabrication and semi-automated characterization of oxide thin film transistors

Yanbing Han(韩炎兵), Sage Bauers, Qun Zhang(张群), Andriy Zakutayev

Chin. Phys. B . 2020, 29(1): 018502 . **doi:** 10.1088/1674-1056/ab5d05

Analysis of non-uniform hetero-gate-dielectric dual-material control gate TFET for suppressing ambipolar nature and improving radio-frequency performance

Hui-Fang Xu(许会芳), Jian Cui(崔健), Wen Sun(孙雯), Xin-Feng Han(韩新风)

Chin. Phys. B . 2019, 28(10): 108501 . **doi:** 10.1088/1674-1056/ab3a8b

Optimization of ambipolar current and analog/RF performance for T-shaped tunnel field-effect transistor with gate dielectric spacer

Ru Han(韩茹), Hai-Chao Zhang(张海潮), Dang-Hui Wang(王党辉), Cui Li(李翠)

Chin. Phys. B . 2019, 28(1): 018505 . **doi:** 10.1088/1674-1056/28/1/018505

Ge/Si heterojunction L-shape tunnel field-effect transistors with hetero-gate-dielectric

Cong Li(李聪), Zhi-Rui Yan(闫志蕊), Yi-Qi Zhuang(庄奕琪), Xiao-Long Zhao(赵小龙), Jia-Min Guo(郭嘉敏)

Chin. Phys. B . 2018, 27(7): 078502 . **doi:** 10.1088/1674-1056/27/7/078502

High-performance inverters based on ambipolar organic-inorganic heterojunction thin-film transistors*

Sheng Sun(孙圣)[1,2], Yuzhi Li(李育智)[1,2], and Shengdong Zhang(张盛东)[1,†]

[1] School of Electronic and Computer Engineering, Peking University Shenzhen Graduate School, Peking University, Shenzhen 518055, China
[2] TCL China Star Optoelectronics Technology Co., Ltd., Shenzhen 518055, China

(Received 27 December 2019; revised manuscript received 20 February 2020; accepted manuscript online 11 March 2020)

This work reports on the integration of organic and inorganic semiconductors as heterojunction active layers for high-performance ambipolar transistors and complementary metal-oxide-semiconductor (CMOS)-like inverters. Pentacene is employed as a p-type organic semiconductor for its stable electrical performance, while the solution-processed scandium (Sc) substituted indium oxide (ScInO) is employed as an n-type inorganic semiconductor. It is observed that by regulating the doping concentration of Sc, the electrical performance of the n-type semiconductor could be well controlled to obtain a balance with the electrical performance of the p-type semiconductor, which is vital for achieving high-performance inverters. When the doping concentration of Sc is 10 at.%, the CMOS-like logic inverters exhibit a voltage gain larger than 80 and a wide noise margin (53% of the theoretical value). The inverters also respond well to the input signal with frequency up to 500 Hz.

Keywords: solution-processed ScInO, ambipolar, transistor, inverter

PACS: 85.30.Pq, 61.82.Fk, 73.40.Lq **DOI:** 10.1088/1674-1056/ab7e96

1. Introduction

Thin-film transistors (TFTs) based on organic and oxide semiconductors have drawn much attention for their potential applications in electronic circuits and displays.[1–5] After years of in-depth studies, the performance of TFTs based on organic and oxide semiconductors has achieved impressive progress, and several groups have demonstrated inverters based on unipolar (p-type or n-type) TFTs.[6–10] To this date, the most studied inverters based on oxide semiconductors consist of two n-type TFTs as a result of lacking high-performance p-type oxide TFTs. These inverters generally have a low voltage gain as they display a weak ability of logic pull-up, and the power consumption of the devices is also significant. The high-performance complementary inverter based on TFTs generally can be fabricated through two different routes. In the first route, the hybrid inverter is obtained through the integration of p-type and n-type TFTs, whereas the other one is the ambipolar inverter based on ambipolar TFTs. Ambipolar TFTs can be constructed based on different structures of the active layer, such as bilayer containing p-type and n-type semiconductors,[11,12] blend of p-type and n-type semiconductors,[13] and bipolar semiconductor.[14,15] Nakanotani *et al.* reported the ambipolar TFTs based on an organic-inorganic hybrid structure containing indium zinc oxide and pentacene bilayer with unbalanced hole and electron mobilities of 0.14 $cm^2 \cdot V^{-1} \cdot s^{-1}$ and 13.8 $cm^2 \cdot V^{-1} \cdot s^{-1}$, respectively.[11] Zhou *et al.* reported flexible ambipolar TFTs based on a solution-processed organic/inorganic heterojunction active layer, but the hole and electron mobilities were inferior (1.2×10^{-2} $cm^2 \cdot V^{-1} \cdot s^{-1}$ and 5.1×10^{-2} $cm^2 \cdot V^{-1} \cdot s^{-1}$, respectively).[16] Luo *et al.* reported high performance inverters base on ambipolar SnO TFTs with passivation of the back-channel surface.[17] Even though ambipolar TFTs based on organic and metal oxide semiconductors have been demonstrated in earlier studies, the performance of such devices is poor, and the switching voltage of the devices cannot be tuned to improve the electrical performance.

Herein, we report a highly stable ambipolar TFT based on organic-inorganic bilayer channel. Pentacene and scandium (Sc) substituted indium oxide (ScInO) were employed as p- and n-type semiconductors, respectively. The electrical performance of ScInO could be easily tuned by adjusting the doping concentration of Sc and thereby accomplishing a balance with the electrical performance of pentacene. Based on the optimized ambipolar TFTs, complementary metal-oxide-semiconductor (CMOS)-like logic inverters were fabricated and they demonstrated excellent switching performance with a high voltage gain larger than 80, a wide noise margin, and an excellent dynamic response.

2. Device fabrication and characterization

2.1. Precursor solutions

ScInO precursors (0.2 M) with different Sc doping concentrations of 2 at.%, 5 at.%, 10 at.%, and 20 at.% were prepared by adding indium nitrate hydrate $[In(NO_3)_3 \cdot xH_2O]$ and

*Project supported by the National Natural Science Foundation of China (Grant Nos. 61574003 and 61774010) and Shenzhen Municipal Scientific Program, China (Grant Nos. GGFW20170728163447038 and JCYJ20180504165449640).

†Corresponding author. E-mail: zhangsd@pku.edu.cn

© 2020 Chinese Physical Society and IOP Publishing Ltd

scandium nitrate hydrate [$Sc(NO_3)_3 \cdot xH_2O$] into deionized (DI) water. The ScInO precursor solutions with the Sc concentrations of 2 at.%, 5 at.%, 10 at.%, and 20 at.% were labeled as ScInO-2, ScInO-5, ScInO-10, and ScInO-20, respectively.

2.2. Devices fabrication

Solution-processed ScInO TFTs were prepared with a bottom-gate, top-contact structure. Firstly, a 300-nm-thick Al:Nd (3 wt.% of Nd) film was deposited on glass substrate via DC sputtering and patterned by the conventional photolithography processes. Then, the Al:Nd film was anodized forming a 200-nm-thick AlO_x:Nd (41 nF·cm^{-2}) layer on the surface. The details of the anodizing processes were reported elsewhere.[18] After 5 min oxygen plasma treatment, the ScInO precursor film was deposited on the AlO_x:Nd film by spin-coating, following which the ScInO precursor film was soft-baked at 50 ℃ for 20 min and then hard-baked at 300 ℃ for 1 h in air. The thickness of the ScInO film was $\sim$ 5 nm. After that, a 220 nm-thick aluminum film was deposited on the ScInO film by thermal evaporation, and passed through the shadow mask as a source electrode and a drain electrode.

For the ambipolar TFTs based on organic-inorganic bilayer channel, after the formation of ScInO layer on AlO_x:Nd film, a 30-nm-thick pentacene film was thermally evaporated onto the ScInO film under a vacuum pressure of $\sim 3 \times 10^{-4}$ Pa with a deposition rate of 0.1 Å·s^{-1}. Then, a 45-nm-thick Au film was thermally evaporated onto the pentacene film through a shadow mask, defining a channel width/length (W/L) of 500 μm/70 μm (as shown in Fig. 1(a)). The fabrication process of the ambipolar inverters and ambipolar TFTs was identical, while the shadow mask for defining the patterns of the Au film for the ambipolar inverters was different (as shown in Fig. 1(b)).

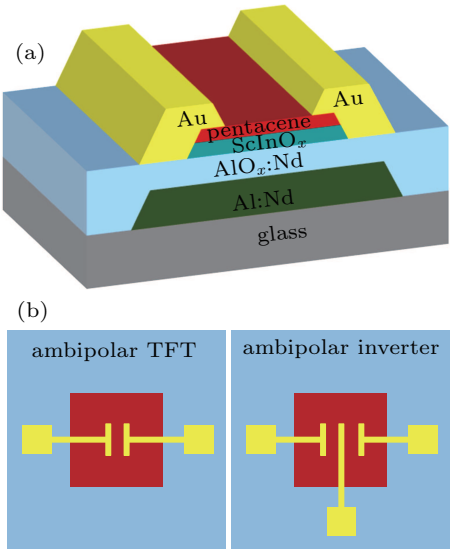


Fig. 1. (a) Schematic diagram of the ambipolar TFTs based on the bilayer structure of pentacene/ScInO. (b) Schematic shows the top-view of the ambipolar TFTs and ambipolar inverters.

2.3. Characterization

The surface morphologies of the ScInO films were measured by an atomic force microscope (AFM, Dimension 3100, Veeco). The electrical properties of the TFTs and inverters were characterized with a semiconductor parameter analyzer (Agilent 4155 C) and a probe station at room temperature (RT) in vacuum environment. To characterize the dynamic response of the fabricated ambipolar inverter, a testing system was constructed, containing a semiconductor analyzer, a function generator, a voltage amplifier, and an oscilloscope. The carrier mobility (μ) of the devices was calculated by the following equation:

$$I_D = \frac{\mu C_i W}{2L}(V_G - V_{th})^2, \quad (1)$$

where C_i is the areal capacitance of the gate insulator, V_G is the gate voltage, and V_{th} is the threshold voltage, which is determined from the conventional linear square root fitting of drain current I_D.[19]

3. Results and discussion

As has been demonstrated in our early work,[20] when the Sc concentration increases, the turn-on voltage (V_{on}) of ScInO TFTs moves in the positive direction, and the off-current decreases, indicating that the free carrier density of the oxide films decreases. Meanwhile, the saturation mobility of the InScO TFTs decreases from 18.4 cm^2·V^{-1}·s^{-1} to 6.4 cm^2·V^{-1}·s^{-1} with an increase in the Sc doping concentration from 2 at.% to 10 at.%. The observed results coincide with the speculation that Sc suppresses the generation of the free carrier.[21,22] The solution-processed In_2O_3 and ScInO thin films based on environmentally-friendly water-induced precursor are quite smooth and uniform. For the ambipolar TFTs based on organic-oxide bilayer channel, the smooth surface of the oxide films offers highly-ordered organic molecule stacking, which is beneficial for the hole transport.[23]

Figure 2 shows the transfer characteristics of the ambipolar TFTs based on pentacene/ScInO bilayer channel. The ambipolar TFTs exhibit an n-channel mode at high positive V_G and a p-channel mode at negative and low positive V_G. As the doping concentration of Sc increases from 0 at.% to 20 at.%, the electron mobility decreases from 4.7 cm^2·V^{-1}·s^{-1} to 0.34 cm^2·V^{-1}·s^{-1}, and simultaneously the hole mobility increases from 0.15 cm^2·V^{-1}·s^{-1} to 0.34 cm^2·V^{-1}·s^{-1}. The V_{th} shows a positive shift with an increase in the doping concentration of Sc. The details of the electrical parameters have been summarized in Table 1. The change in mobility and threshold voltage could be ascribed to a decrease in the carrier concentration in the ScInO films with an increase in the doping concentration of Sc.

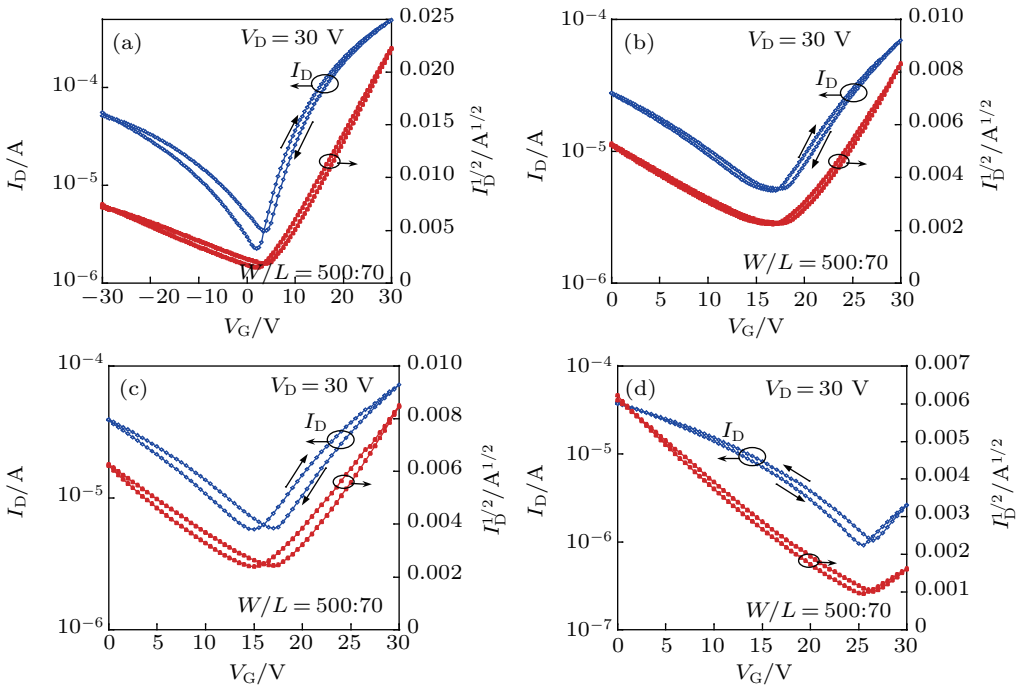


Fig. 2. The transfer characteristics of ambipolar TFTs with various doping concentrations of Sc: (a) 0 at.%, (b) 5 at.%, (c) 10 at.%, (d) 20 at.%.

Table 1. The electrical parameters of the ambipolar TFTs and inverters.

Sc/at.%	μ/cm^2·V^{-1}·s^{-1}		V_{th}/V		V_{SW} of the inverters at third quadrant/V	
	N-type	P-type	N-type	P-type	Calculated	Experimental
0	4.7	0.15	5	−27	−26.0	−22.5
5	2.7	0.31	15	−10	−13.4	−15.5
10	1.9	0.43	17	−12	−12.3	−14.5
20	0.34	0.34	22	−7	−7.5	−5.6

To explore the feasibility of the ambipolar TFTs applying in inverters, CMOS-like inverters are fabricated by integrating two ambipolar TFTs. Figure 3(a) shows the voltage transfer curves (VTCs) of the inverters based on ambipolar TFTs with different doping concentrations of Sc. As the supply voltage (V_{DD}) of −30 V is biased to the inverters, the output voltage (V_{OUT}) varies from low to high in response to the input voltage (V_{IN}) sweeping from high to low. In the low/high V_{IN} regions, V_{OUT} is lower/higher than 0 V/−30 V, owing to incomplete off-state of the ambipolar transistors. Figures 3(a) and 3(b) show that the switching voltage (V_{SW}) and voltage gain vary for the ambipolar inverters with different doping concentrations of Sc. According to the quadratic model of the metal-oxide semiconductor transistors, the V_{SW} at the first quadrant is given by

$$V_{SW}^{ambi} = \frac{V_{DD} + V_{TP} + V_{TN}\sqrt{\mu_N}/\mu_P}{1 + \sqrt{\mu_N}/\mu_P}, \tag{2}$$

while V_{SW} at the third quadrant is given by

$$V_{SW}^{ambi} = \frac{V_{DD} + V_{TN} + V_{TP}\sqrt{\mu_P}/\mu_N}{1 + \sqrt{\mu_P}/\mu_N}, \tag{3}$$

where V_{TP} and V_{TN} are the threshold voltages of p-channel and n-channel of the ambipolar TFTs, respectively; μ_P and μ_N are the hole mobility and electron mobility of the ambipolar TFTs, respectively.[24,25] The above equations reveal that the V_{SW} of the CMOS-like inverters can be tuned by adjusting V_{TP}, V_{TN}, μ_P, and μ_N of the ambipolar TFTs.

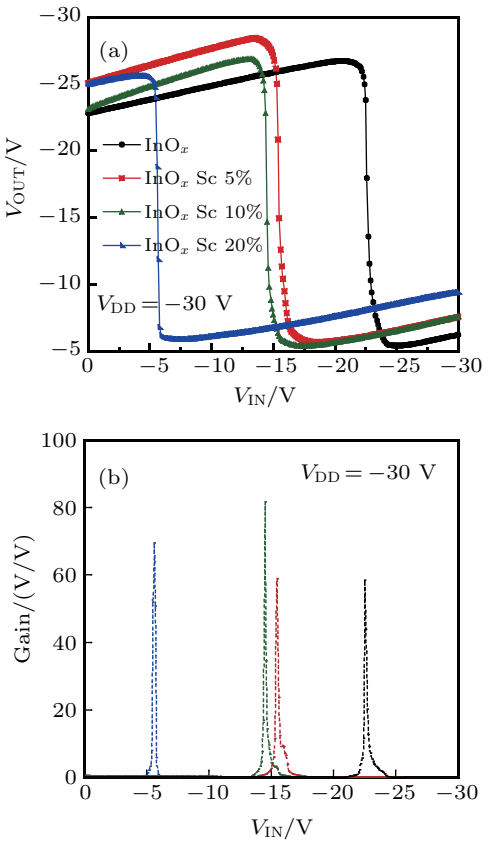


Fig. 3. (a) The voltage transfer curve and (b) the corresponding voltage gain of CMOS-like inverters based on ambipolar TFTs with various doping concentrations of Sc under $V_{DD} = -30$ V.

Generally, to obtain high voltage gain and wide noise margin (NM) for the CMOS-like inverters, the V_{SW} should be tuned close to the midpoint of V_{DD} ($V_{DD}/2$). As shown in Table 1, the CMOS-like inverters employing ScInO-10 films as n-channel exhibit an experimental V_{SW} (-14.5 V) near $V_{DD}/2$, and the device also presents a maximum voltage gain of 81.6 (see Fig. 3(b)), indicating the balanced transfer characteristics of the n-channel and p-channel modes in the ambipolar TFTs. The extracted electrical properties are summarized in Table 2. The input-low voltage (V_{IL}) and the input-high voltage (V_{IH}) are the input voltages at the point of $dV_{OUT}/dV_{IN} = -1$, while the output-high voltage (V_{OH}) and the output-low voltage (V_{OL}) are the output voltages for $V_{IN} = V_{IL}$ and V_{IH}, respectively. The high noise margin ($NM_H = V_{OH} - V_{IH}$) is calculated as 8.0 V, which is 53.3% of $V_{DD}/2$, and the low noise margin ($NM_L = V_{IL} - V_{OL}$) is 9.1 V, which is about 60.7% of $V_{DD}/2$. Large noise margin provides strong immunity to interference and avoids logic errors. This is essential for the reliable operation of large scale integrated circuits. Generally, a noise margin above 30% is necessary for the inverter. The inverter in this study shows a good noise margin, which is superior to the already reported unipolar inverters. The transition width ($\Delta V_{IN} = V_{IH} - V_{IL}$) is 0.73 V, indicating that the CMOS-like inverter can be rapidly switched between V_{OL} and V_{OH}. The excellent performance of the fabricated inverter could be attributed to its excellent and balanced ambipolar electrical characteristics.

Table 2. Electrical properties of CMOS-like inverter operating at $V_{DD} = -30$ V.

V_{SW}/V	V_{OH}/V	V_{IH}/V	V_{IL}/V	V_{OL}/V	NM_H/V	NM_L/V	ΔV_{IN}/V
−14.5	−5.9	−13.9	−15.7	−26.8	8.0	9.1	0.73

Figure 4 shows that the CMOS-like inverters can operate at the third quadrant too. The device presents a maximum voltage gain of 75, the NM_H and NM_L are estimated to be 12.8 V and 12.6 V. It is the unique feature of the inverter based on ambipolar TFTs among all kinds of inverters because the ambipolar TFTs can work at positive and negative biases.

The dynamic characteristics of the inverter refer to its response to the pulse input signal, which is as important as the static characteristics. To test the dynamic characteristics of the CMOS-like inverters, a dynamic response testing system was built. Figure 5 shows the dynamic response of the CMOS-like inverters at various input signal frequencies. It can be seen clearly that the devices respond well for the input signal frequency lower than 100 Hz. When the input signal frequency goes up to 500 Hz, the output signal has a little delay because the effect of parasitic capacity becomes more obvious. The transit frequency (f_T) is a figure of merit to characterize the operation speed of TFT, which is defined as

$$f_T \approx \frac{\mu (V_G - V_{th})}{4\pi L^2} \frac{C_{ch}}{C_{ch} + C_p}, \tag{4}$$

where L is the channel length, C_{ch} is the channel capacitance, and C_p is the parasitic overlap capacitance.[26] It is expected that shortening the L to submicron scale and reducing the C_p can greatly improve the dynamic response of the CMOS-like inverters.

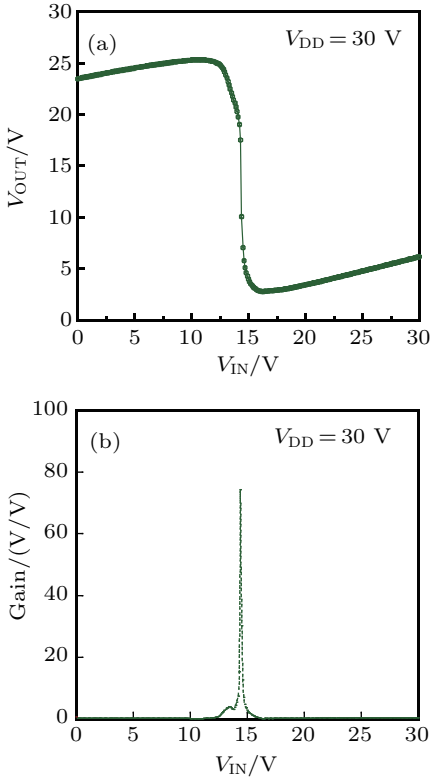


Fig. 4. (a) The voltage transfer curve and (b) the corresponding voltage gain under $V_{DD} = 30$ V.

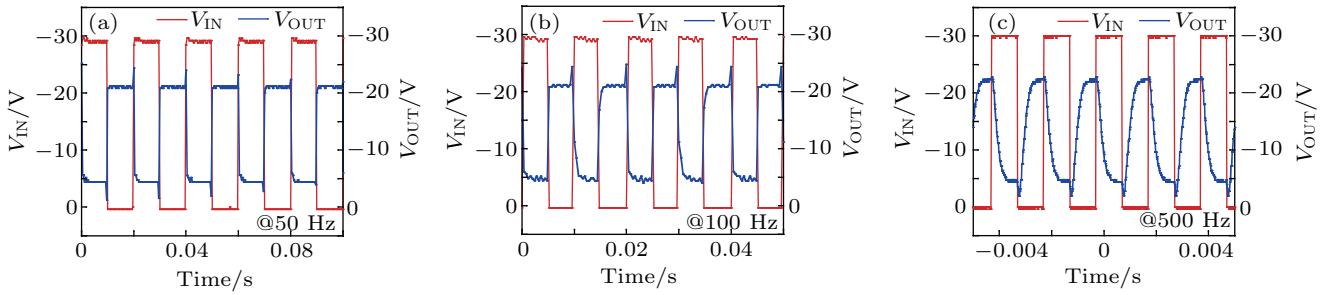


Fig. 5. The dynamic response of the CMOS-like inverters at the input signal frequencies of (a) 50 Hz, (b) 100 Hz, (c) 500 Hz.

4. Conclusion

In summary, ambipolar TFTs and CMOS-like inverters are fabricated based on pentacene/ScInO heterojunction active layers. The performance of the devices can be tuned by adjusting the doping concentrations of Sc in the ScInO films. With the optimized Sc doping concentration of 10 at.%, the constructed CMOS-like inverters exhibit a voltage gain of 81.6 at V_{DD} of −30 V, a large noise margin, and an excellent dynamic response to the input signal with frequency up to 500 Hz. Overall, this study paves the way for further research, whereby it can be expected that ambipolar inverters with superior performance can be found in the near future.

References

[1] Nomura K, Ohta H, Takagi A, Kamiya T, Hirano M and Hosono H 2004 *Nature* **432** 488

[2] Fortunato E M C, Barquinha P M C, Pimentel A C M B G, Goncalves A M F, Marques A J S, Pereira L M N and Martins R F P 2005 *Adv. Mater.* **17** 590

[3] Song K, Noh J, Jun T, Jung Y, Kang H Y and Moon J 2010 *Adv. Mater.* **22** 4308

[4] Liu Y R, S J, Lai P T and Yao R H 2014 *Chin. Phys. B* **23** 068501

[5] Micjan M, Novota M, Telek P, Donoval M and Weis M 2019 *Chin. Phys. B* **28** 118501

[6] Li J, Zhong D Y, Huang C X, Li X F and Zhang J H 2018 *IEEE Trans. Electron. Devices* **65** 2838

[7] Orlandi M O 2020 *Tin Oxide Materials-Synthesis, Properties, and Applications* (Amsterdam: Elsevier) p. 441

[8] Smith J, Bashir A, Adamopoulos G, Anthony J E, Bradley D D C, Heeney M, McCulloch I and Anthopoulos T D 2010 *Adv. Mater.* **22** 3598

[9] Yang C, Kwack Y, Kim S H, An T K, Hong K, Nam S, Park M, Choi W S and Park C E 2011 *Org. Electron.* **12** 411

[10] Yang J, Wang Y M, Li Y P, Yuan Y Z, Hu Z J, Ma P F, Zhou L, Wang Q P, Song A M and Xin Q 2018 *IEEE Electron Device Lett.* **39** 516

[11] Nakanotani H, Yahiro M, Adachi C and Yano K 2007 *Appl. Phys. Lett.* **90** 262104

[12] Guo X J, Feng L R, Cui Q Y and Xu X L 2014 *IEEE Electron Device Lett.* **35** 542

[13] Opitz A, Bronner M, Brütting W, Himmerlich M, Schaefer J A and Krischok S 2007 *Appl. Phys. Lett.* **90** 212112

[14] Anthopoulos T D, Setayesh S, Smits E, Cölle M, Cantatore E, de B Blom P W M and de D M 2006 *Adv. Mater.* **18** 1900

[15] Bisri S Z, Piliego C, Gao J and Loi M A 2014 *Adv. Mater.* **26** 1176

[16] Zhou Y, Han S T, Zhou L, Yan Y, Huang L B, Huang J and Roy V A L 2013 *J. Mater. Chem. C* **1** 7073

[17] Luo H, Liang L Y, Cao H T, Dai M Z, Lu Y C and Wang M 2015 *ACS Appl. Mater. Inter.* **7** 17023

[18] Lan L F, Zhao M J, Xiong N N, Xiao P, Shi W, Xu M and Peng J B 2012 *IEEE Electron Device Lett.* **33** 827

[19] Brotherton S D 2013 *Introduction to Thin Film Transistors* (Heidelberg: Springer) p. 46

[20] Song W, Lan L F, Li M L, Wang L, Lin Z G, Sun S, Li Y Z, Song E L, Gao P X, Li Y and Peng J B 2017 *J. Phys. D: Appl. Phys.* **50** 385108

[21] Song W, Lan L F, Xiao P, Lin Z G, Sun S and Peng J B 2016 *IEEE Trans. Electron. Devices* **63** 4315

[22] Choi Y, Kim G H, Jeong W H, Bae J H, Kim H J, Hong J M and Yu W J 2010 *Appl. Phys. Lett.* **97** 162102

[23] Steudel S, Vusser S D, Jonge S D, Janssen D, Verlaak S, Genoe J and Heremans P 2004 *Appl. Phys. Lett.* **85** 4400

[24] Risteska A, Chan K Y, Anthopoulos T D, Gordijn A, Stiebig H, Nakamura M and Knipp D 2012 *Org. Electron.* **13** 2816

[25] Baeg K J, Caironi M and Noh Y Y 2013 *Adv. Mater.* **25** 4210

[26] Klauk H 2010 *Chem. Soc. Rev.* **39** 2643